Supporting Information

Halogenated sodium/lithium monocarba-*closo*-decaborates: syntheses, characterization, and solid-state ionic conductivity

Shouhu Li,[a] Pengtao Qiu,*[a] Jia-xin Kang,[a] Zhenpu Shi,[b] Yichun Zhang,[a] Yiming Ma[a] and Xuenian Chen*[a,c]

[a] Henan Key Laboratory of Boron Chemistry and Advanced Energy Materials, School of Chemistry and Chemical Engineering, Henan Normal University, Xinxiang, Henan 453007, China

[b] School of Chemistry and Chemical Engineering, Henan Normal University, Xinxiang, Henan 453007, China

[c] Green Catalysis Center and College of Chemistry, Zhengzhou University, Zhengzhou, Henan 450001, China

NMR spectra (Figures S1-S5) of Na[*closo*-1-CHB_9H_8-6-Br]:

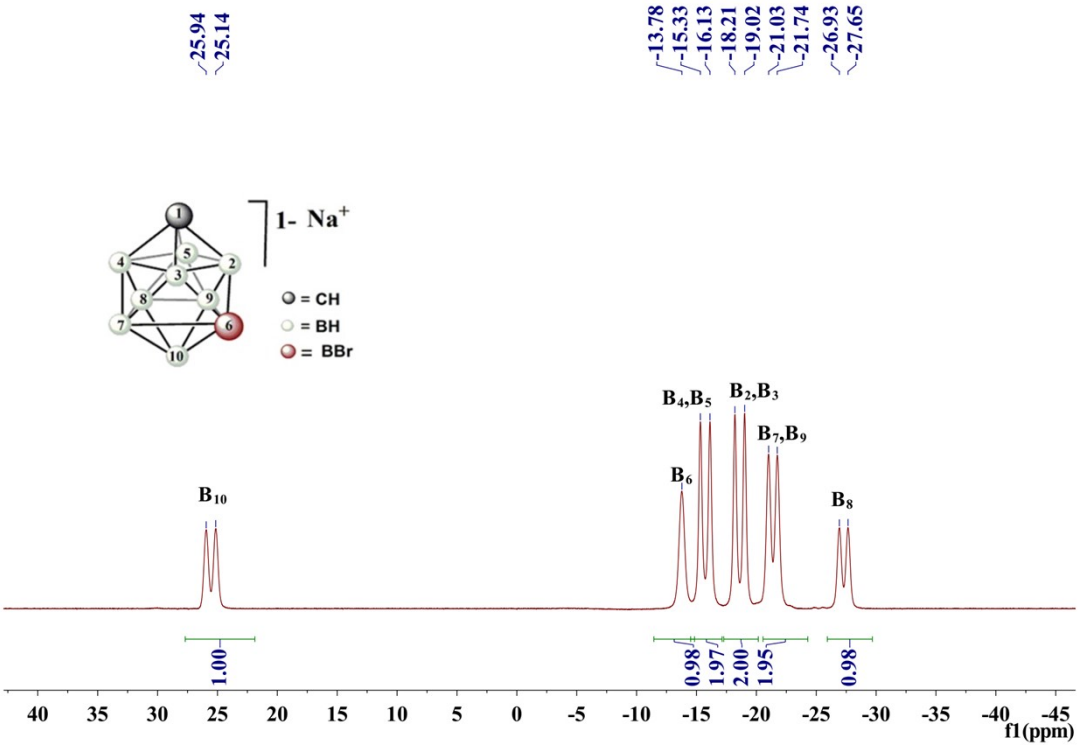

Figure S1. ^{11}B NMR spectrum of Na[*closo*-1-CHB_9H_8-6-Br] in D_2O

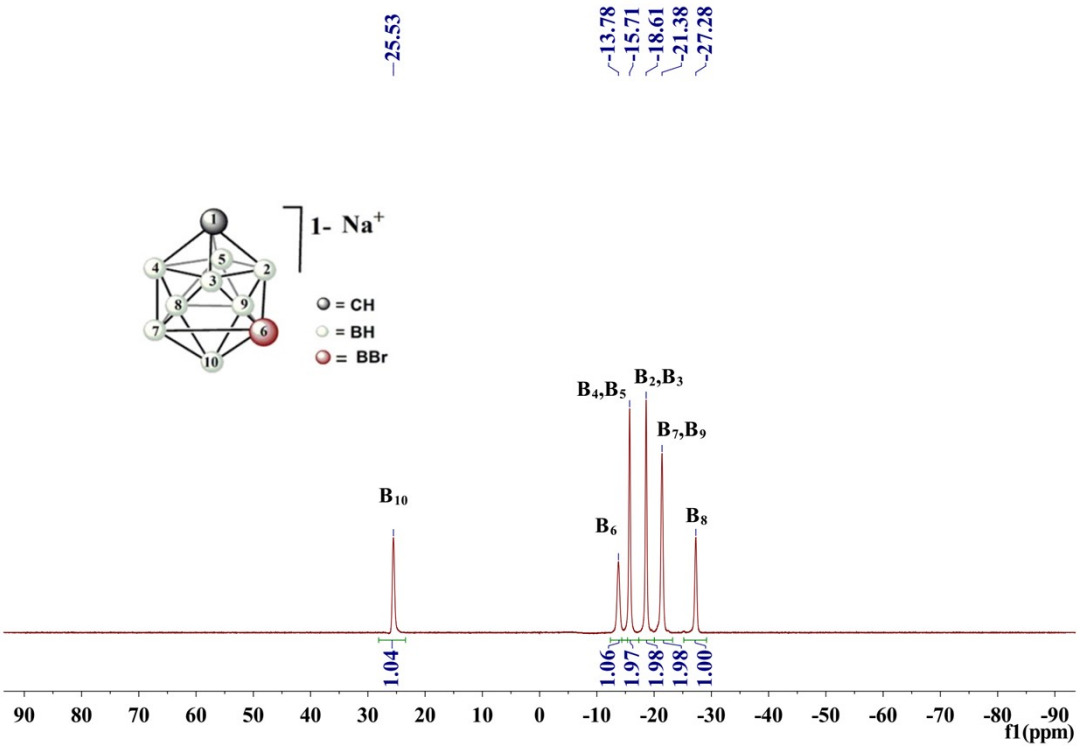

Figure S2. $^{11}B\{^1H\}$ NMR spectrum of Na[*closo*-1-CHB_9H_8-6-Br] in D_2O

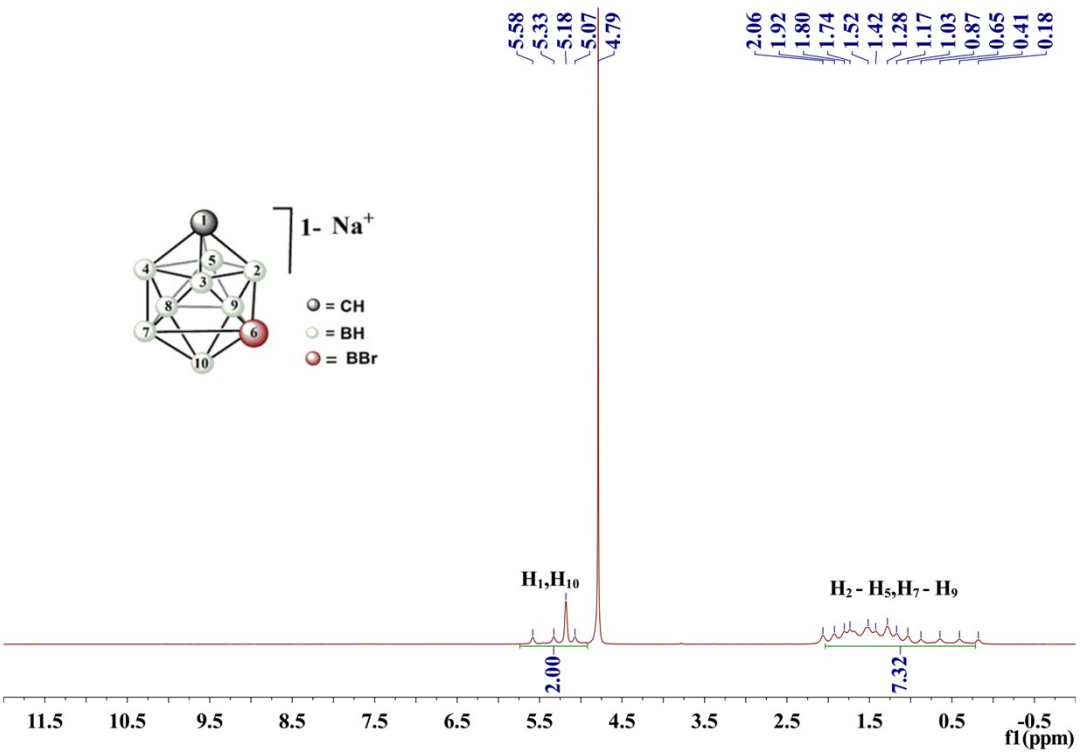

Figure S3. ^{1}H NMR spectrum of Na[*closo*-1-CHB_9H_8-6-Br] in D_2O

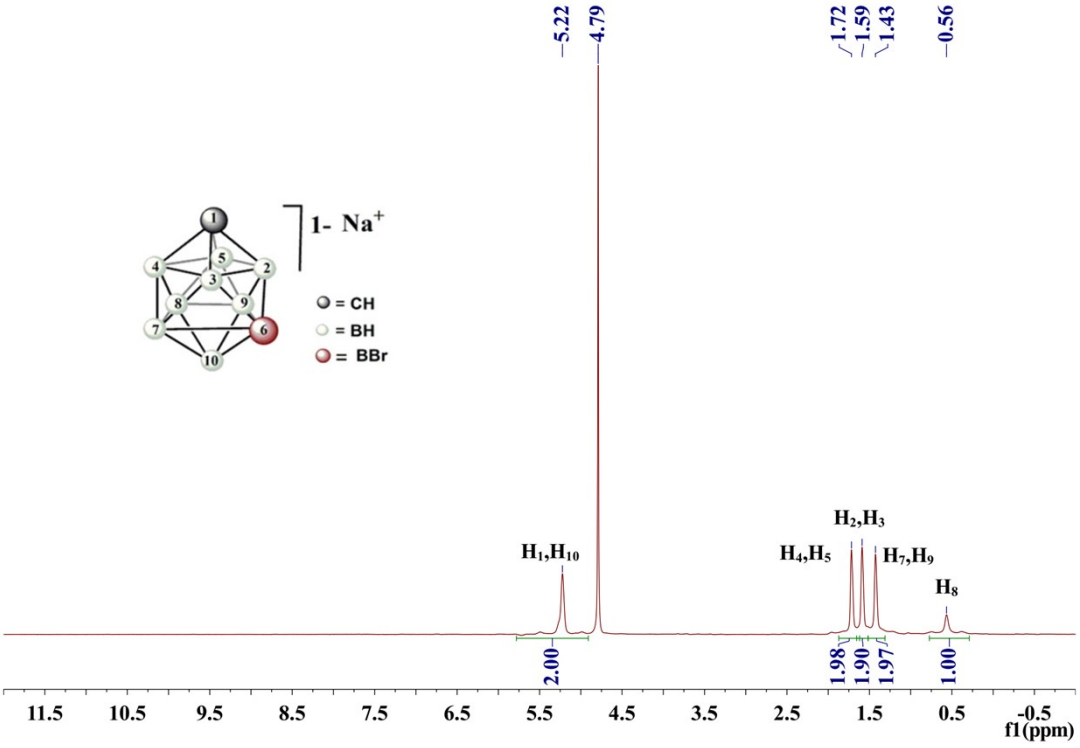

Figure S4. $^{1}H\{^{11}B\}$ NMR spectrum of Na[*closo*-1-CHB_9H_8-6-Br] in D_2O

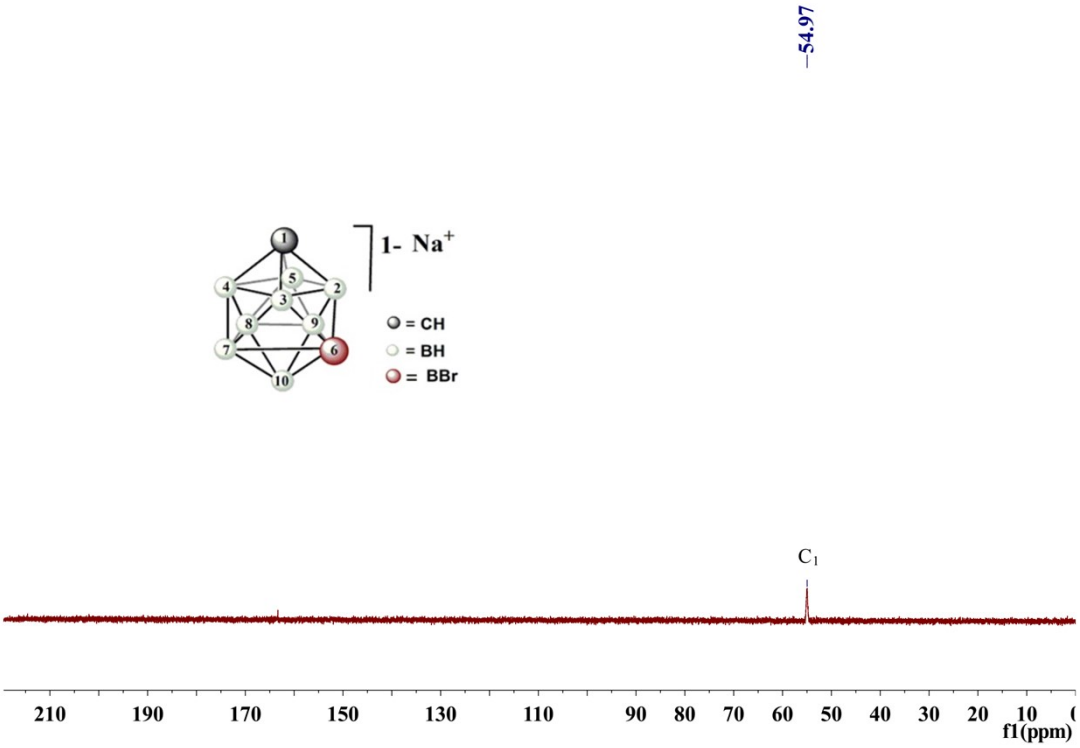

Figure S5. ^{13}C NMR spectrum of Na[*closo*-1-CHB_9H_8-6-Br] in D_2O

NMR spectra (Figure S6-S10) of Na[*closo*-1-CHB_9H_8-6-I]:

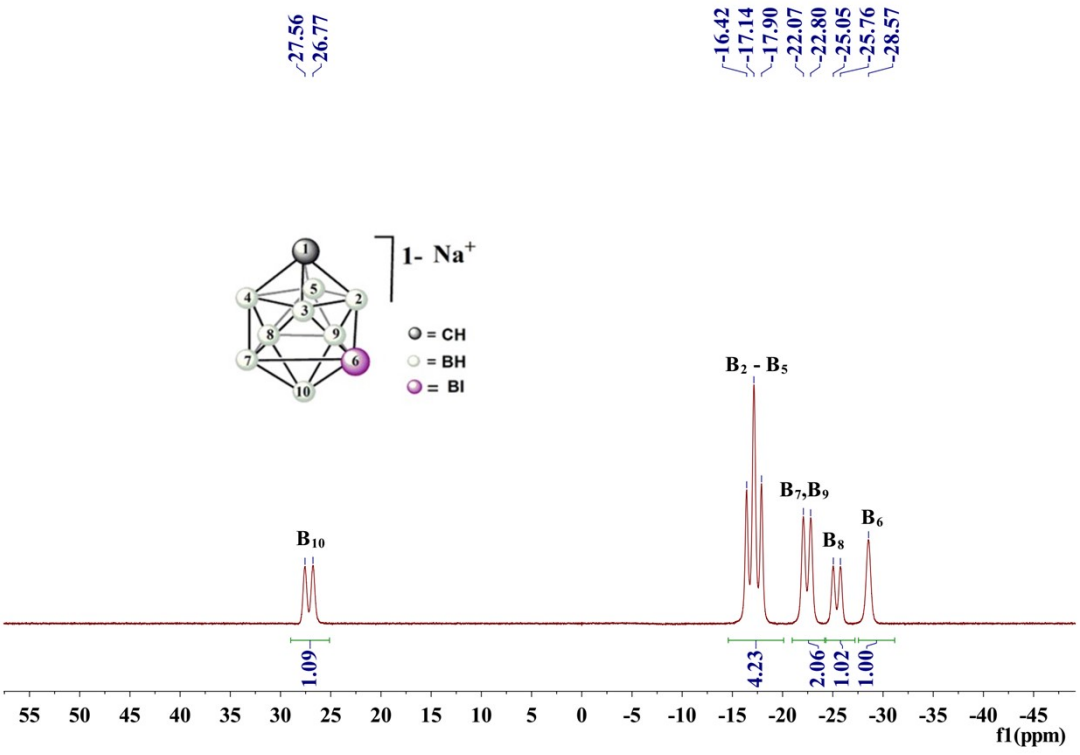

Figure S6.^{11}B NMR spectrum of Na[*closo*-1-CHB_9H_8-6-I] in D_2O

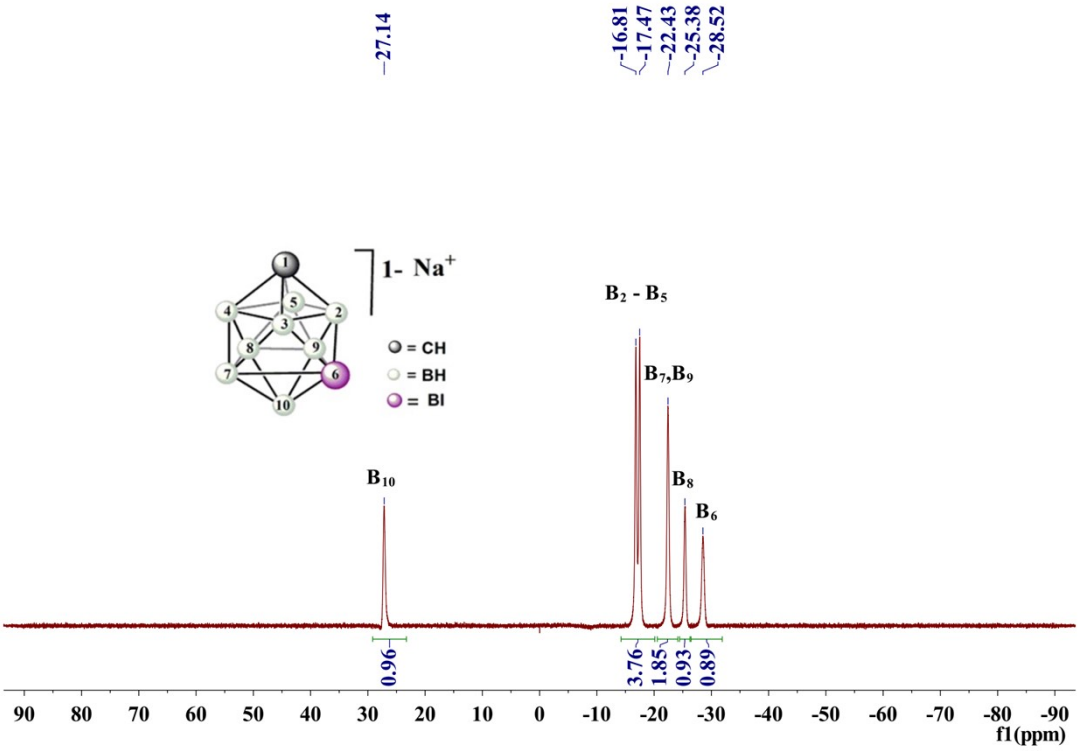

Figure S7. $^{11}B\{^{1}H\}$ NMR spectrum of Na[*closo*-1-CHB_9H_8-6-I] in D_2O

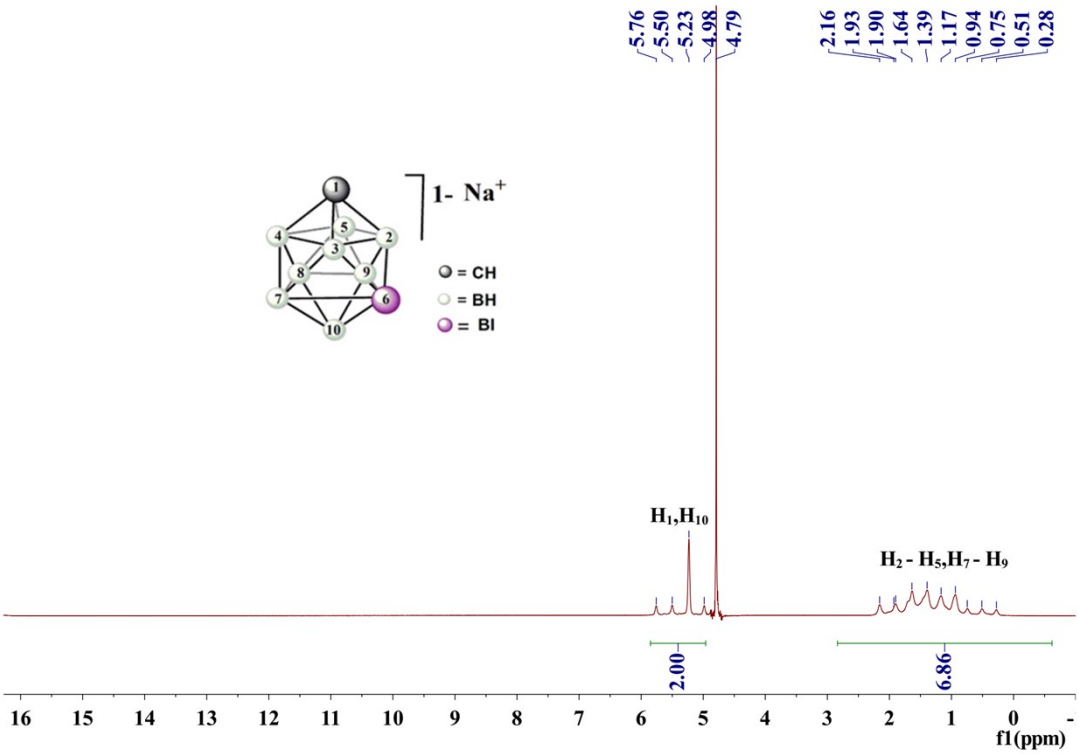

Figure S8. ^{1}H NMR spectrum of Na[*closo*-1-CHB_9H_8-6-I] in D_2O

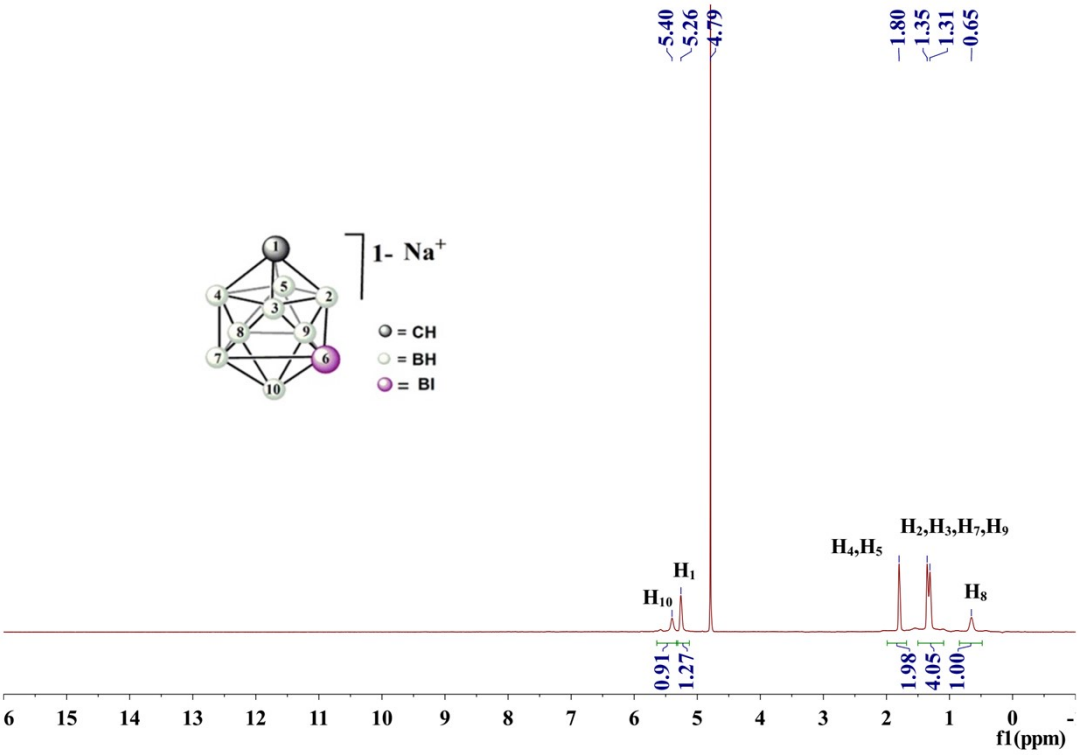

Figure S9. $^{1}H\{^{11}B\}$ NMR spectrum of Na[*closo*-1-CHB_9H_8-6-I] in D_2O

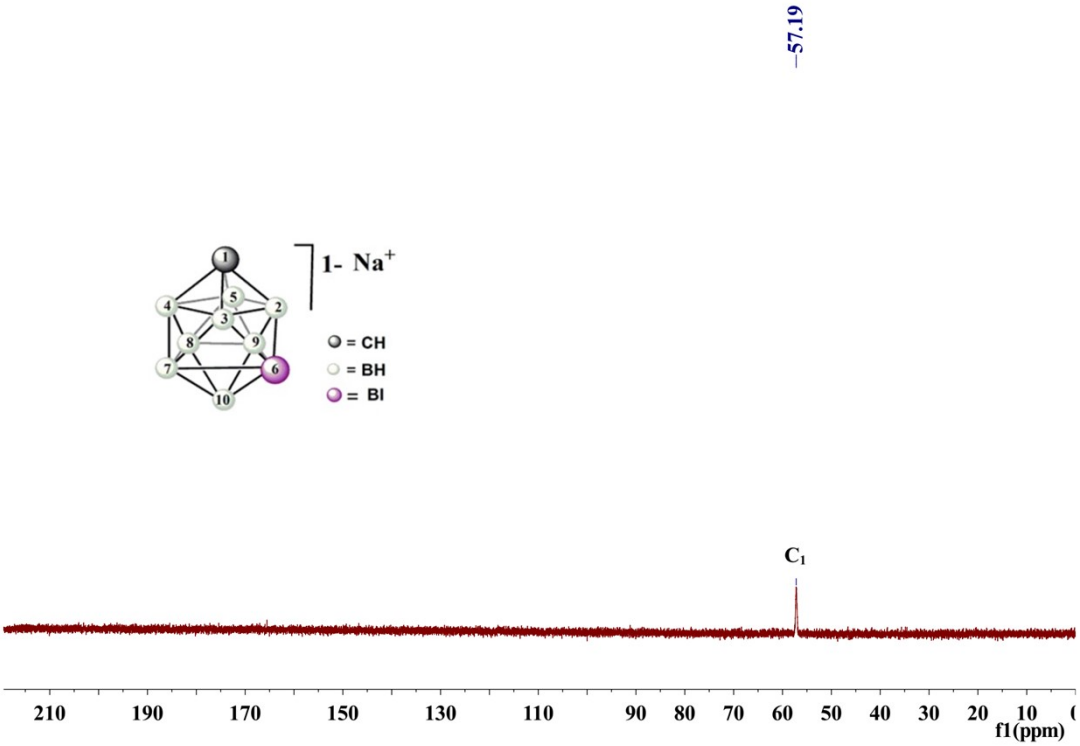

Figure S10. ^{13}C NMR spectrum of Na[*closo*-1-CHB_9H_8-6-I] in D_2O

NMR spectra (Figures S11-S15) of Na[*closo*-1-CHB_9H_4-6,7,8,9,10-I_5]:

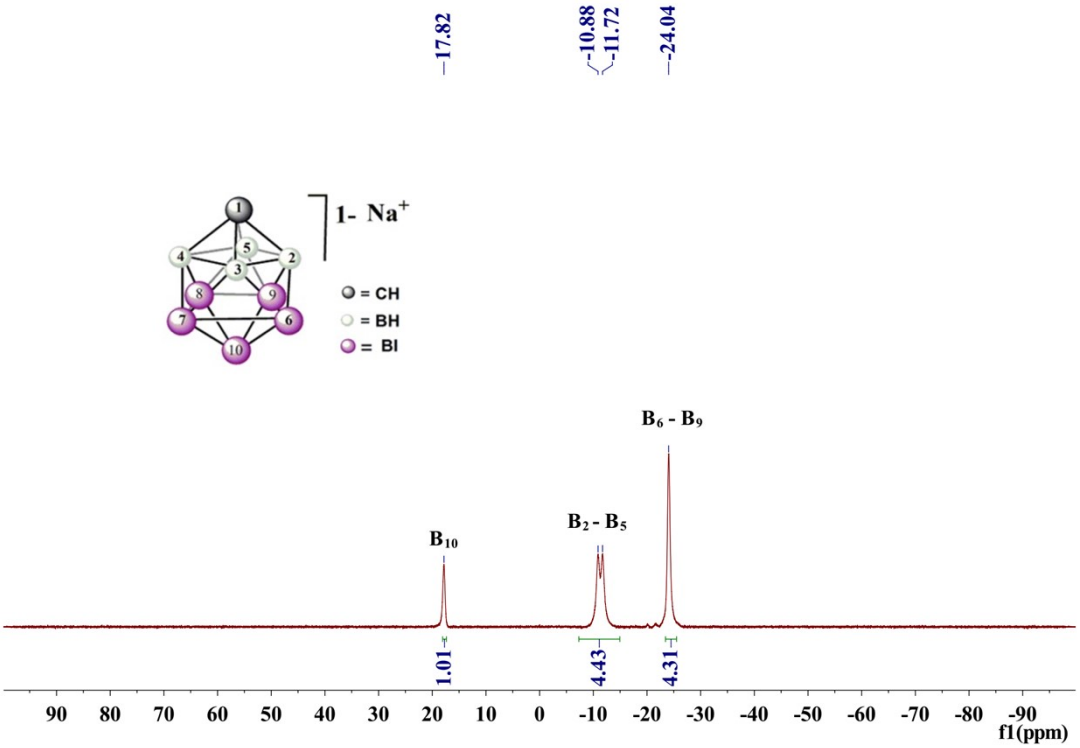

Figure S11. ^{11}B NMR spectrum of Na[*closo*-1-CHB_9H_4-6,7,8,9,10-I_5] in D_2O

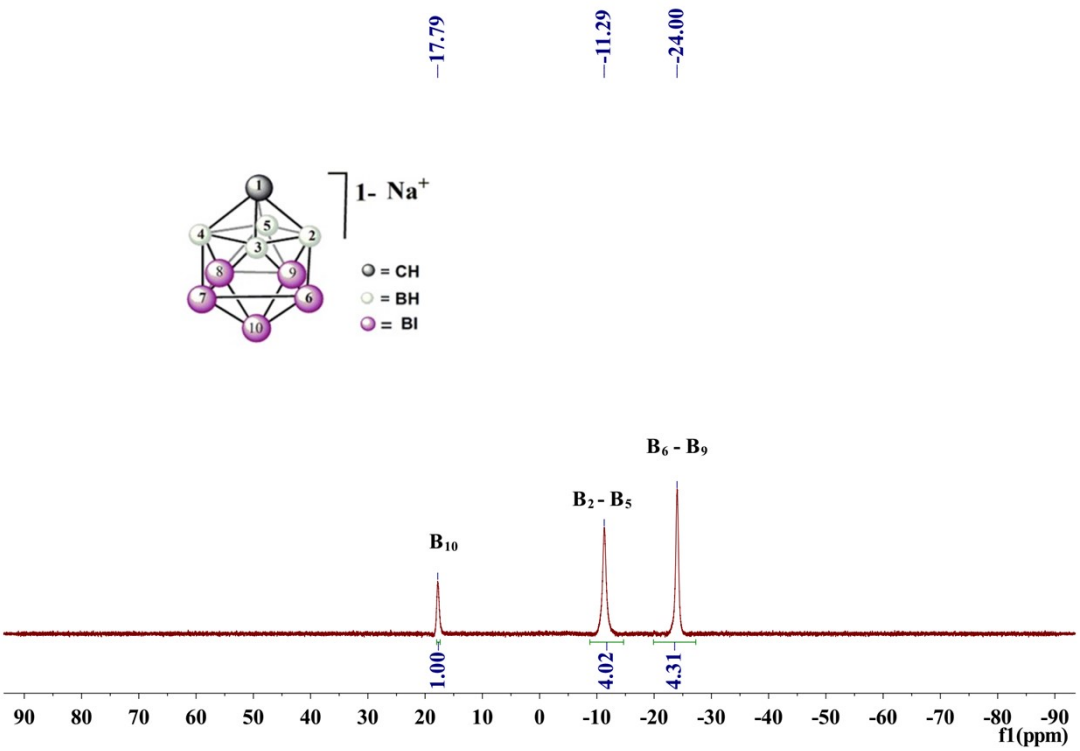

Figure S12. $^{11}B\{^1H\}$ NMR spectrum of Na[*closo*-1-CHB_9H_4-6,7,8,9,10-I_5] in D_2O

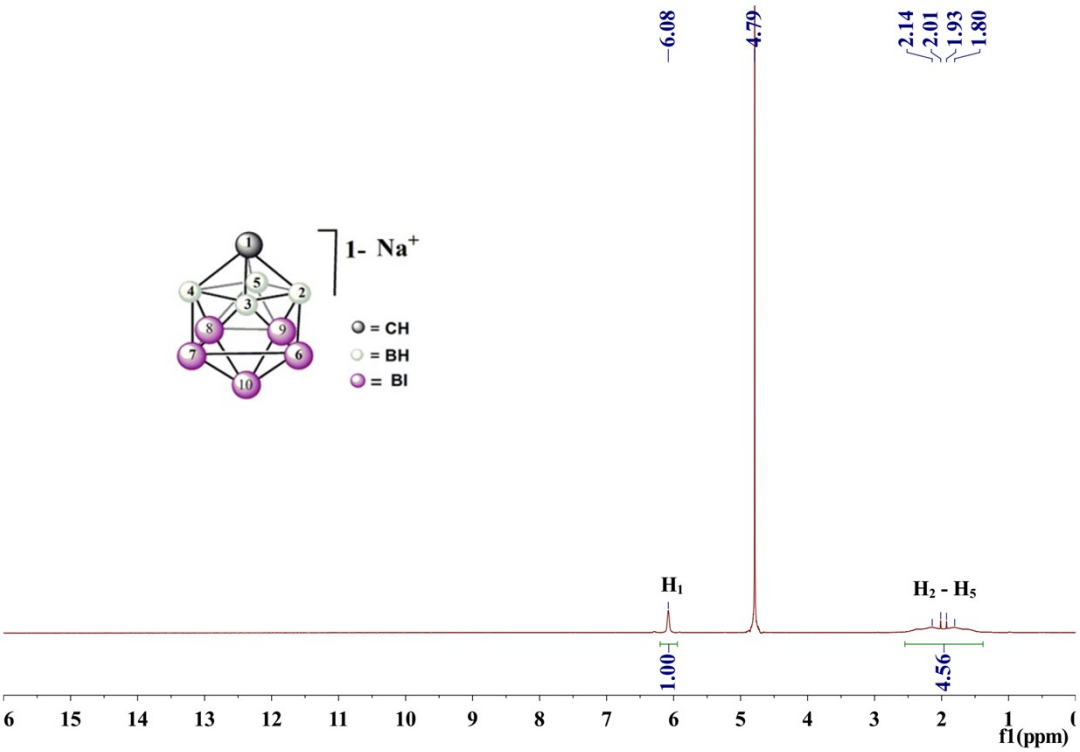

Figure S13. ^{1}H NMR spectrum of Na[*closo*-1-CHB_9H_4-6,7,8,9,10-I_5] in D_2O

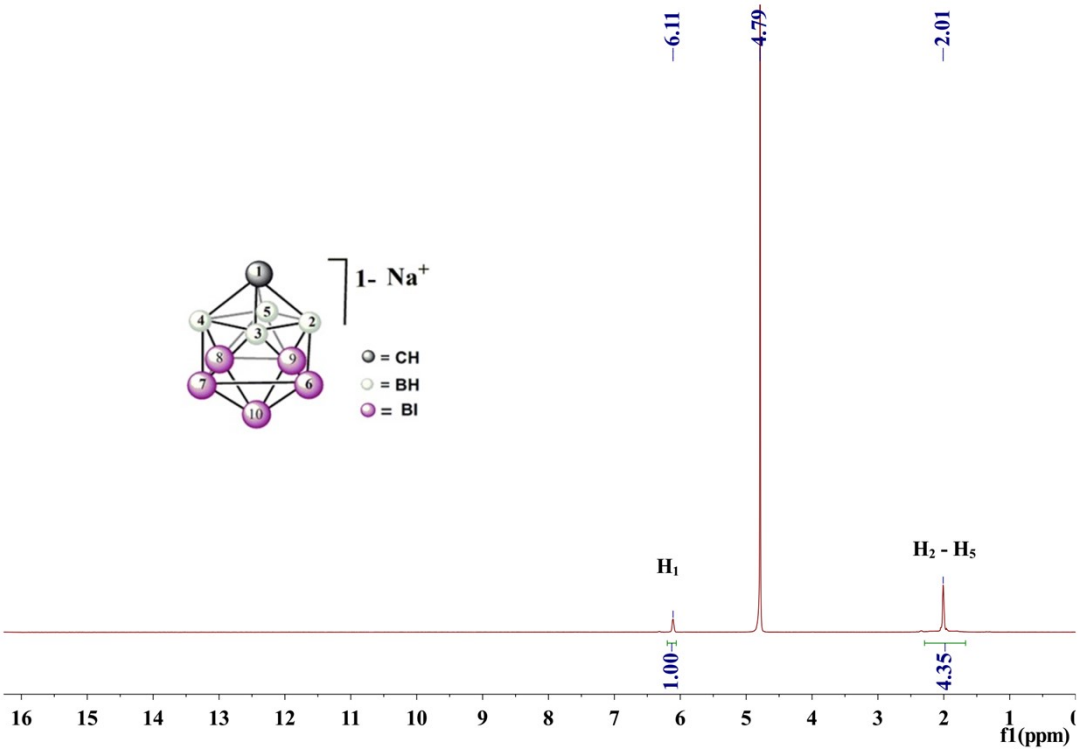

Figure S14. $^{1}H\{^{11}B\}$ NMR spectrum of Na[*closo*-1-CHB_9H_4-6,7,8,9,10-I_5] in D_2O

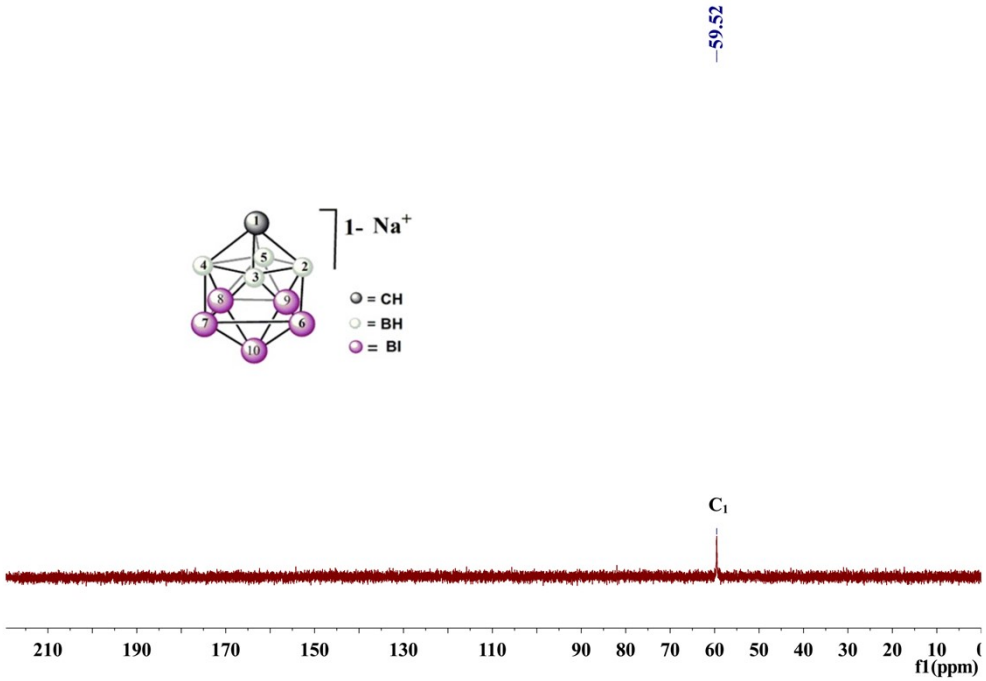

Figure S15. ^{13}C NMR spectrum of Na[*closo*-1-CHB_9H_4-6,7,8,9,10-I_5] in D_2O

NMR spectra (Figures S16-S20) of Li[*closo*-1-CHB_9H_8-6-Br]:

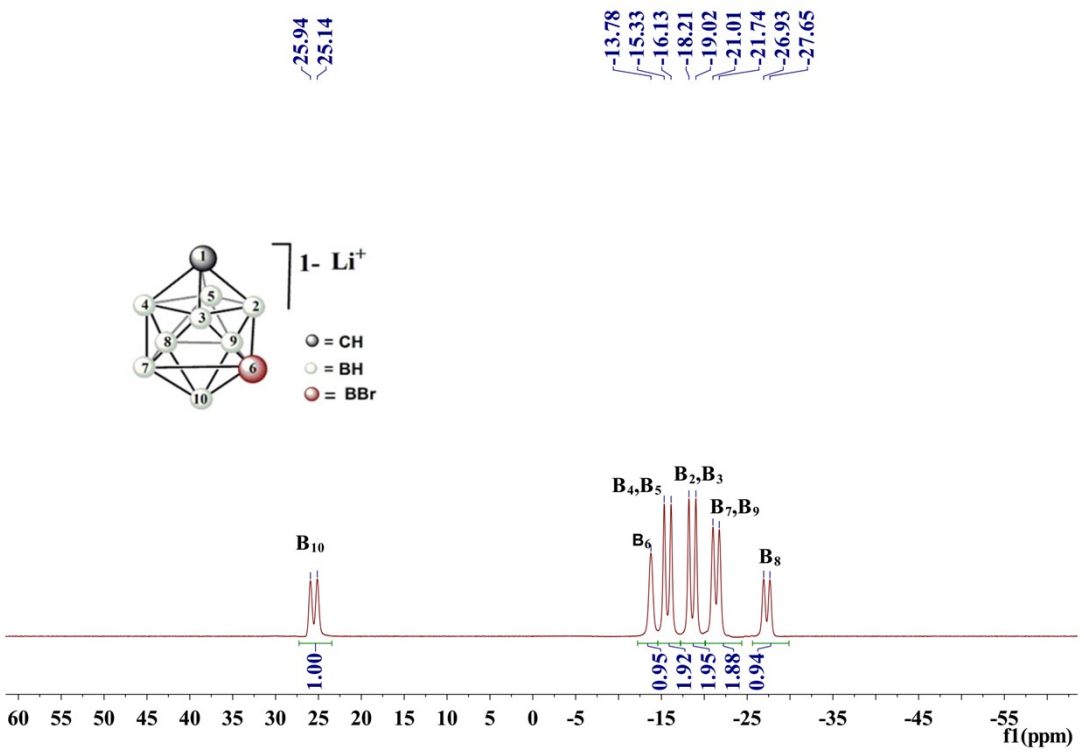

Figure S16. ^{11}B NMR spectrum of Li[*closo*-1-CHB_9H_8-6-Br] in D_2O

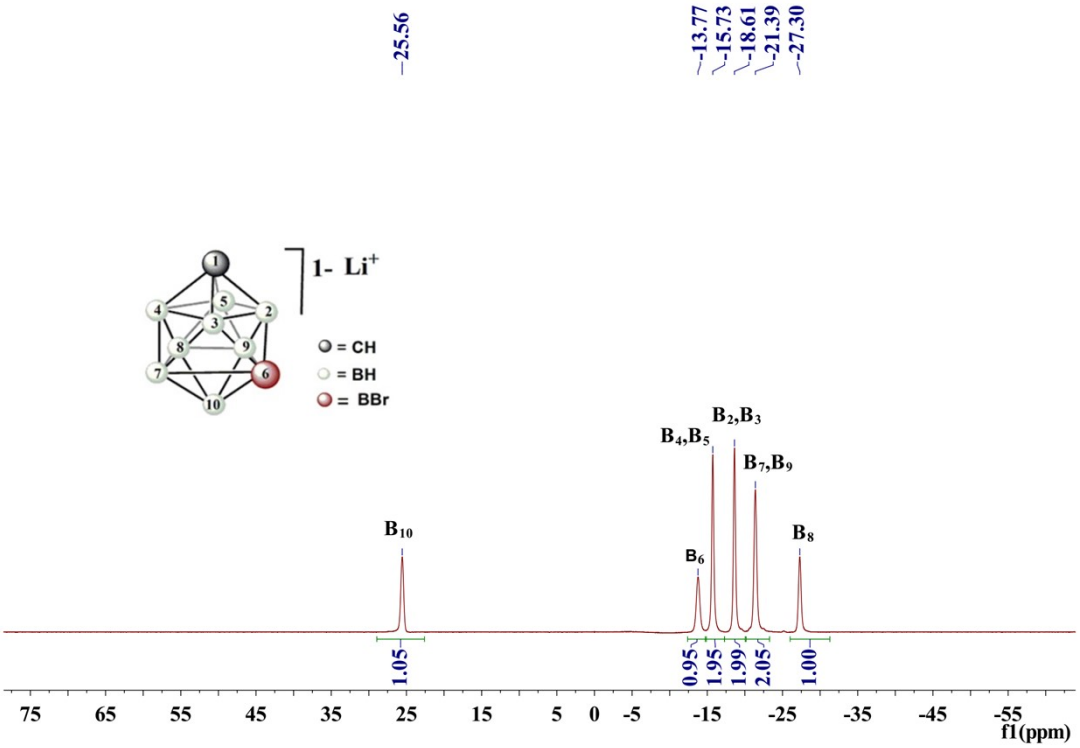

Figure S17. $^{11}B\{^{1}H\}$ NMR spectrum of Li[*closo*-1-CHB_9H_8-6-Br] in D_2O

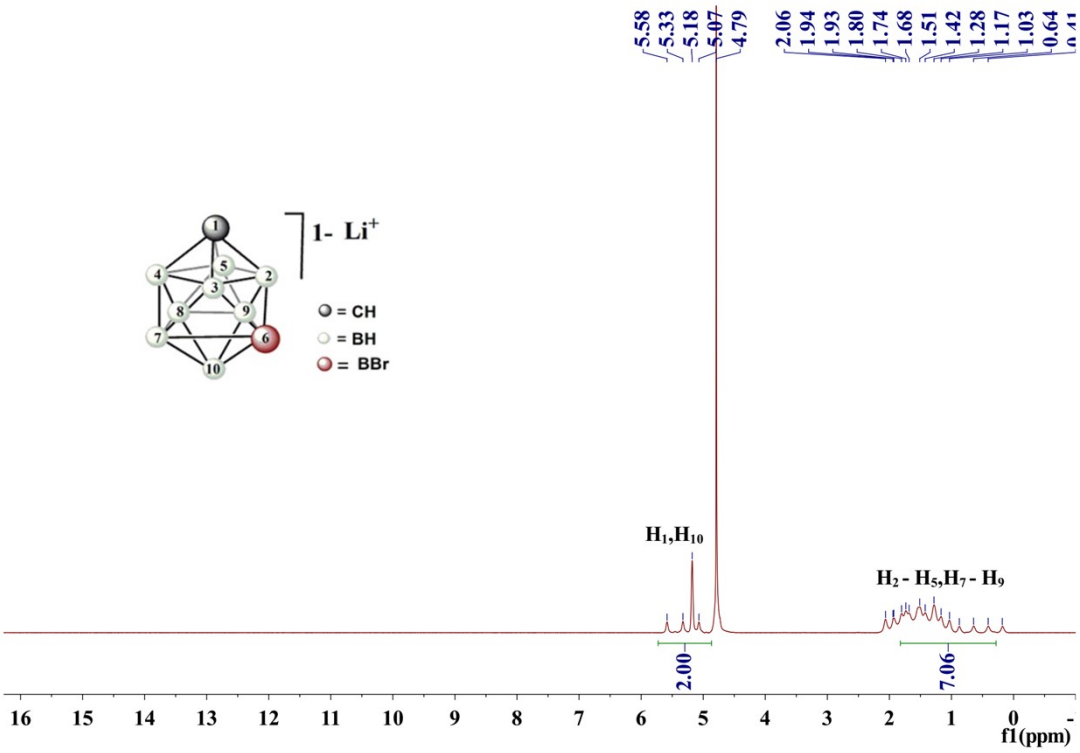

Figure S18. ^{1}H NMR spectrum of Li[*closo*-1-CHB_9H_8-6-Br] in D_2O

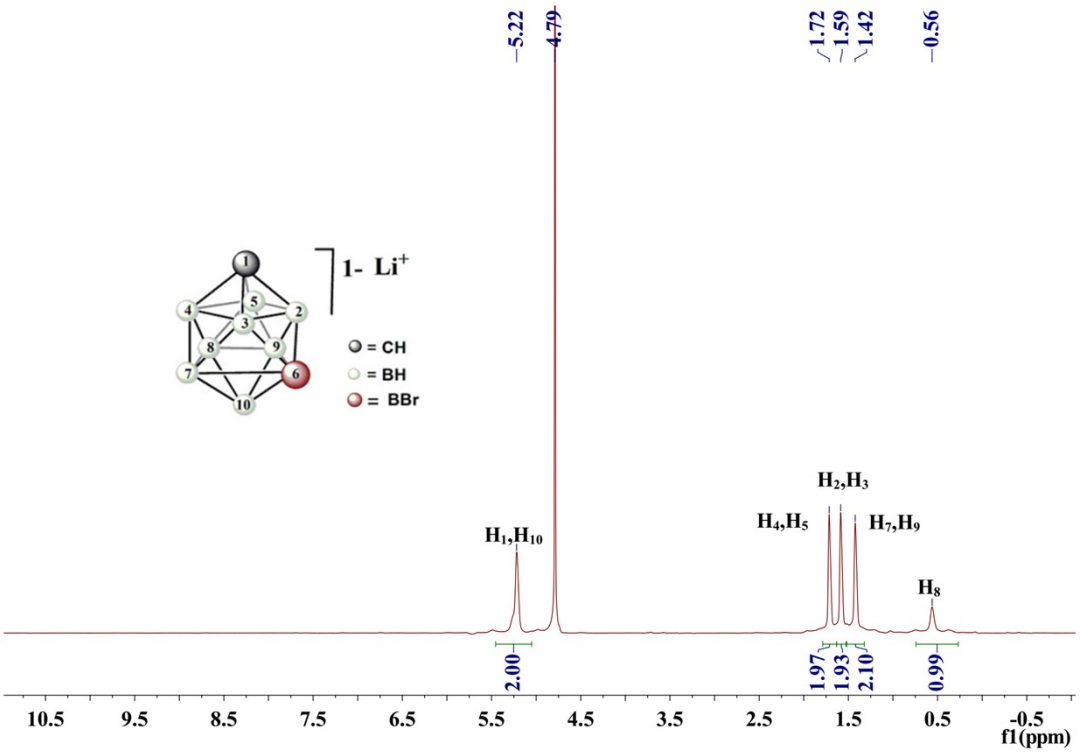

Figure S19. $^{1}H\{^{11}B\}$ NMR spectrum of Li[*closo*-1-CHB_9H_8-6-Br] in D_2O

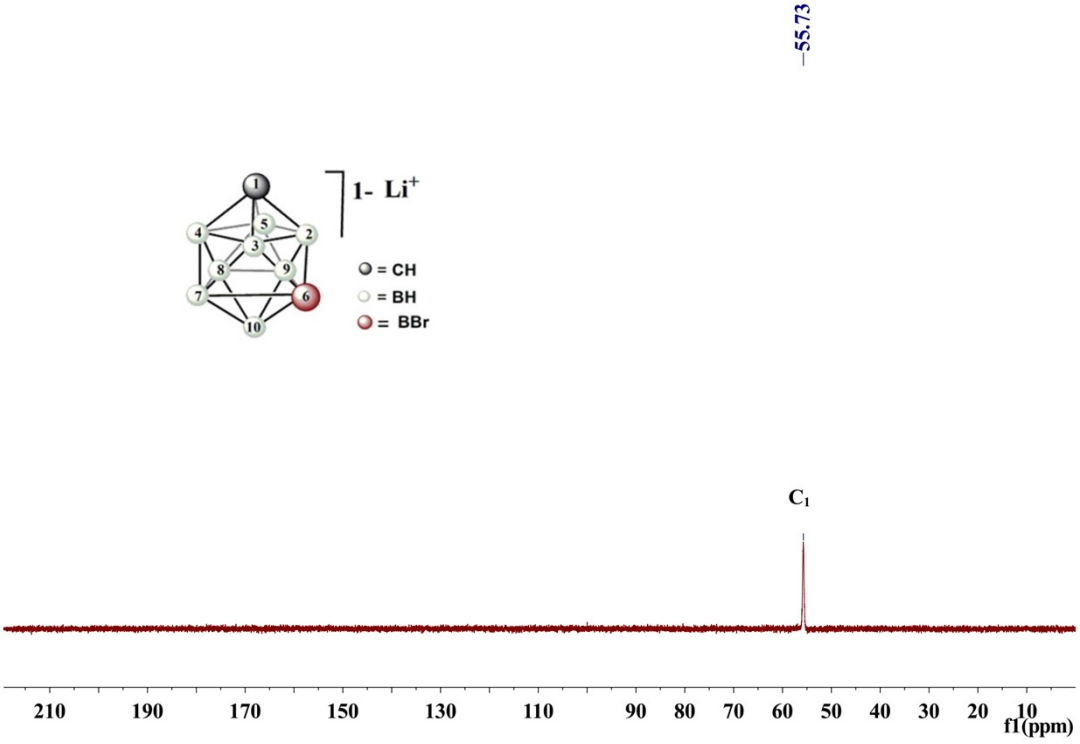

Figure S20. ^{13}C NMR spectrum of Li[*closo*-1-CHB_9H_8-6-Br] in D_2O

NMR spectra (Figures S21-S25) of Li[*closo*-1-CHB_9H_8-6-I]:

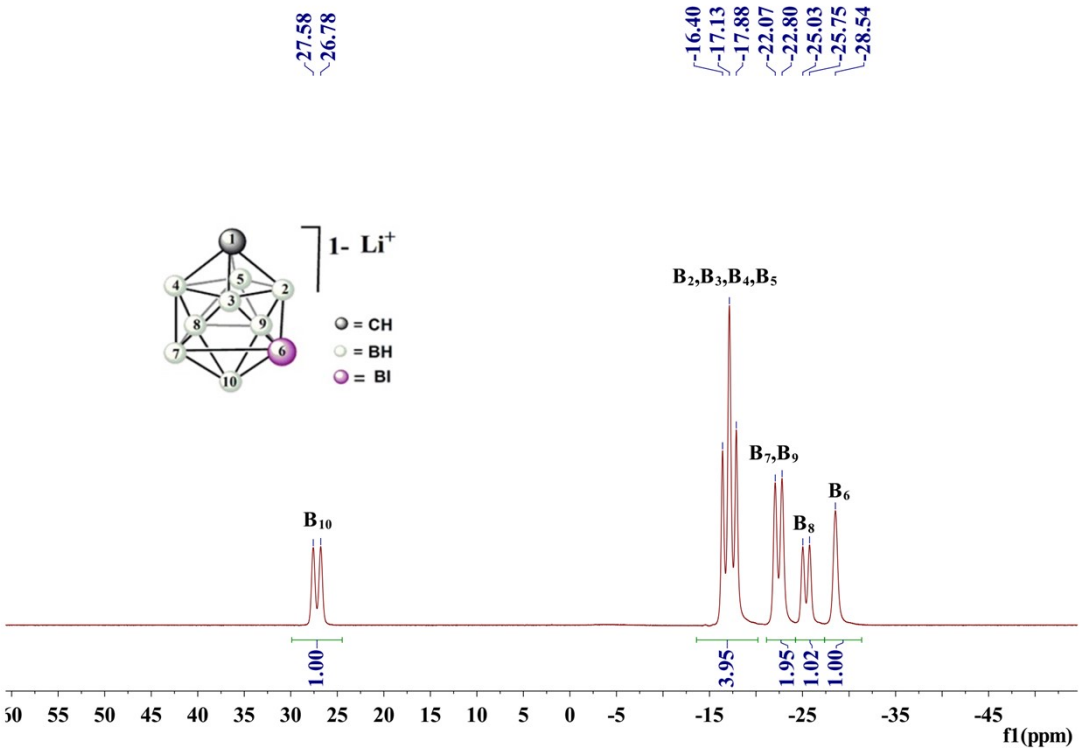

Figure S21. ^{11}B NMR spectrum of Li[*closo*-1-CHB_9H_8-6-I] in D_2O

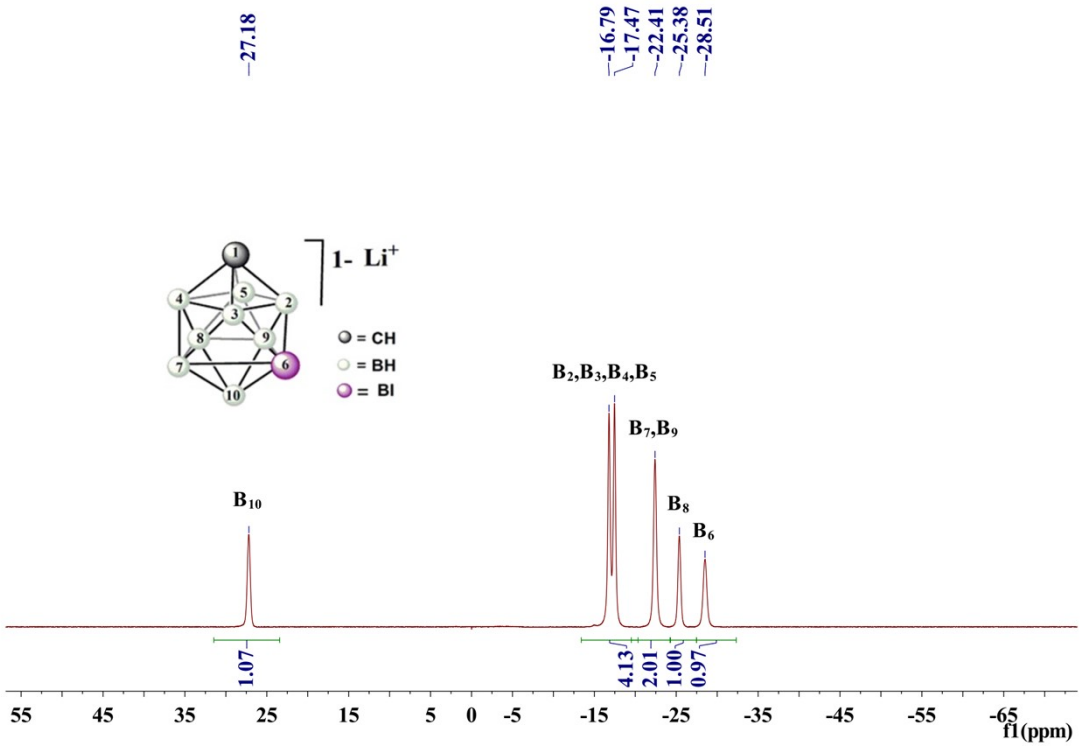

Figure S22. $^{11}B\{^1H\}$ NMR spectrum of Li[*closo*-1-CHB_9H_8-6-I] in D_2O

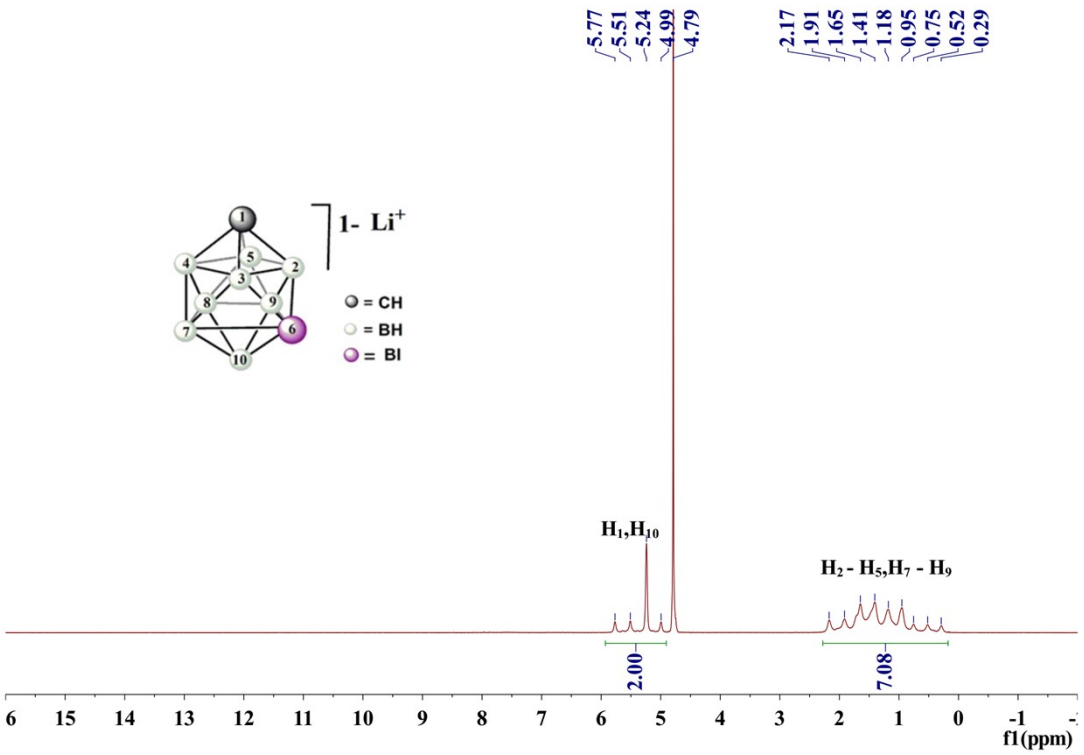

Figure S23. ^{1}H NMR spectrum of Li[*closo*-1-CHB_9H_8-6-I] in D_2O

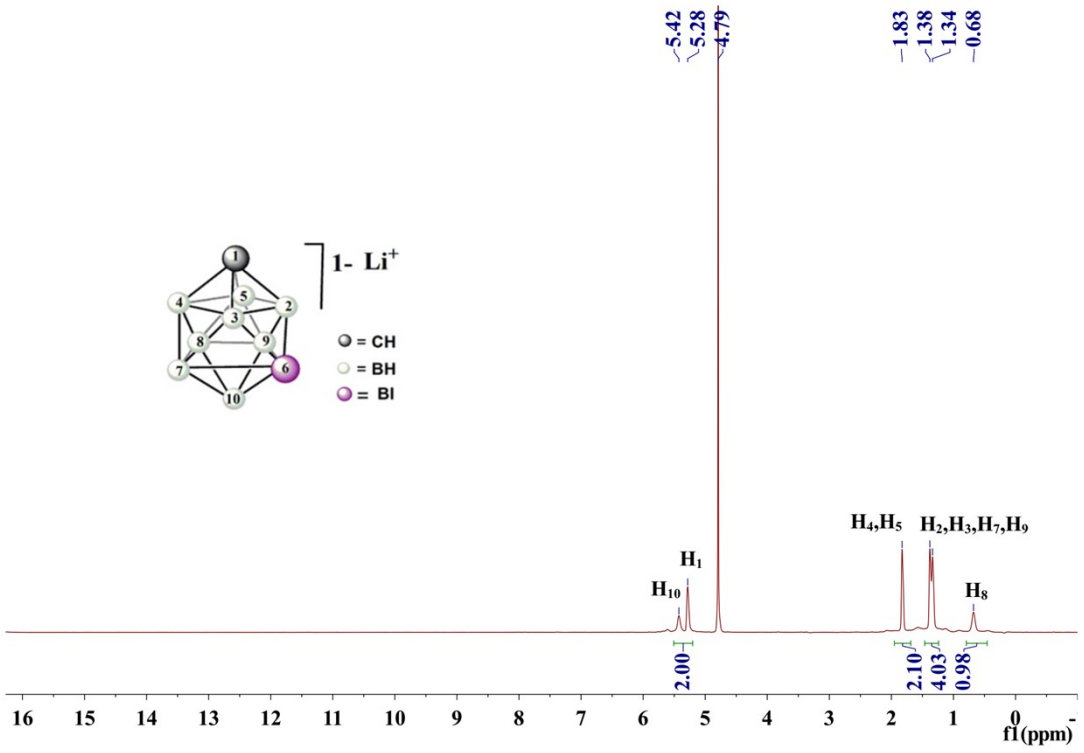

Figure S24. $^{1}H\{^{11}B\}$ NMR spectrum of Li[*closo*-1-CHB_9H_8-6-I] in D_2O

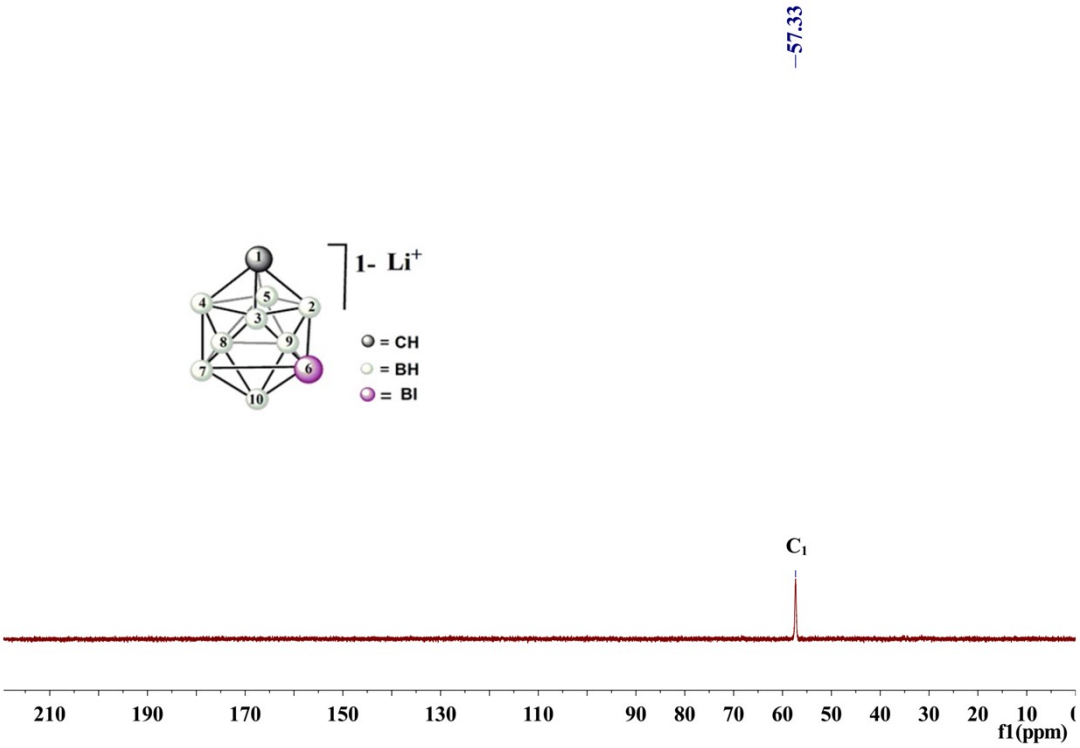

Figure S25. ^{13}C NMR spectrum of Li[*closo*-1-CHB_9H_8-6-I] in D_2O

NMR spectra (Figures S26-S30) of Li[*closo*-1-CHB_9H_4-6,7,8,9,10-I_5]:

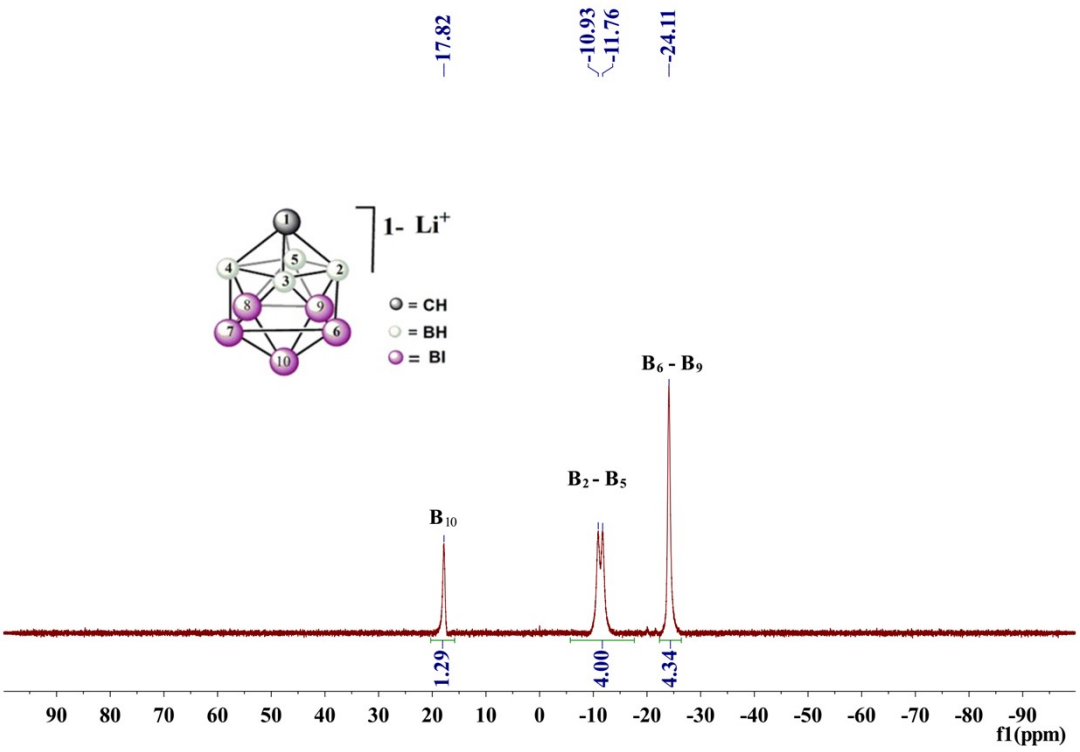

Figure S26. ^{11}B NMR spectrum of Li[*closo*-1-CHB_9H_4-6,7,8,9,10-I_5] in D_2O

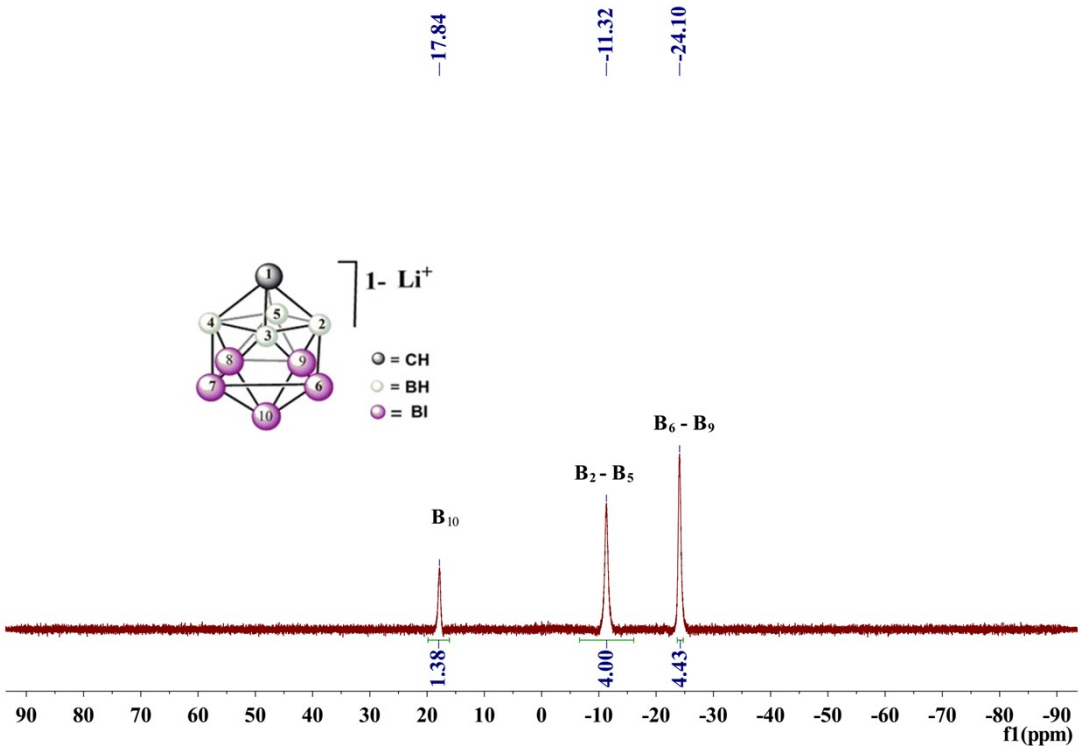

Figure S27. $^{11}B\{^{1}H\}$ NMR spectrum of Li[*closo*-1-CHB_9H_4-6,7,8,9,10-I_5] in D_2O

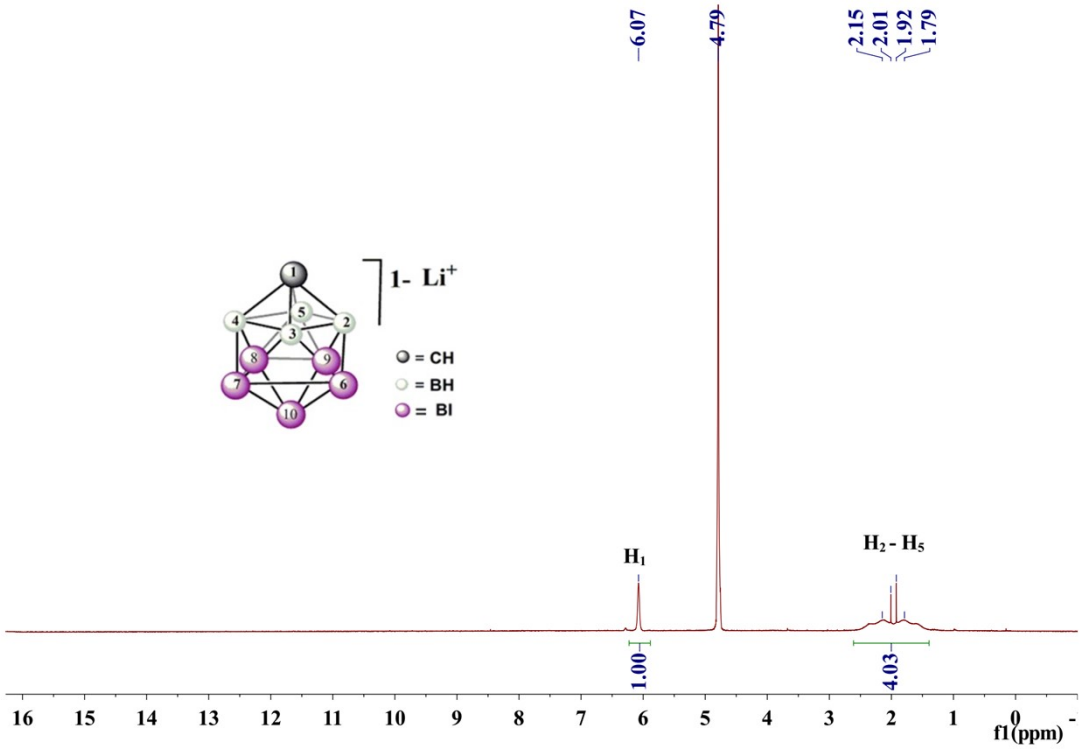

Figure S28. ^{1}H NMR spectrum of Li[*closo*-1-CHB_9H_4-6,7,8,9,10-I_5] in D_2O

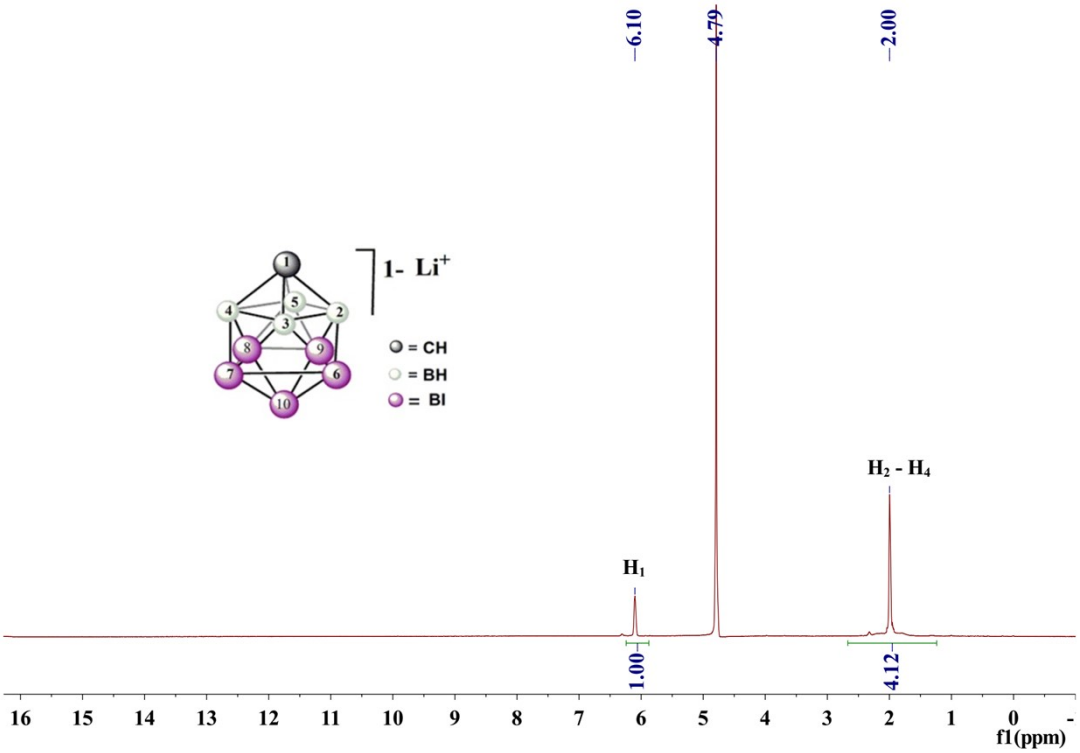

Figure S29. $^{1}H\{^{11}B\}$ NMR spectrum of Li[*closo*-1-CHB_9H_4-6,7,8,9,10-I_5] in D_2O

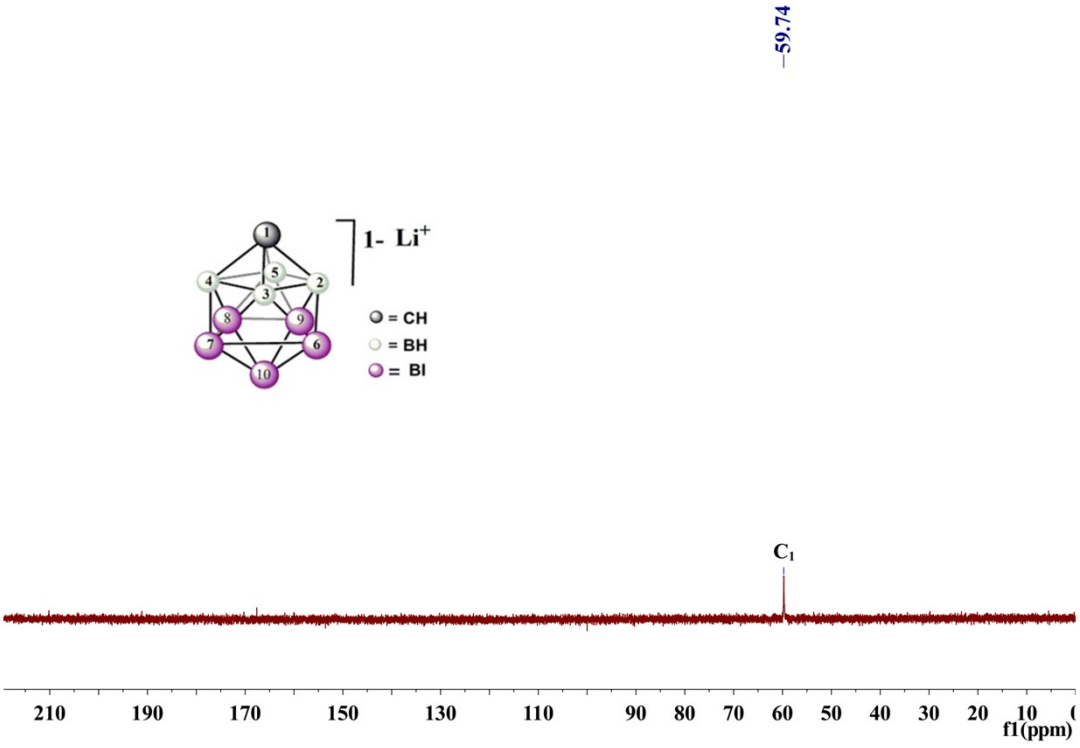

Figure S30. ^{13}C NMR spectrum of Li[*closo*-1-CHB_9H_4-6,7,8,9,10-I_5] in D_2O

Mass spectra for M[*closo*-1-CHB_9H_8-6-Br], M[*closo*-1-CHB_9H_8-6-I], M[*closo*-1-CHB_9H_4-6,7,8,9,10-I_5] (M = Na, Li)

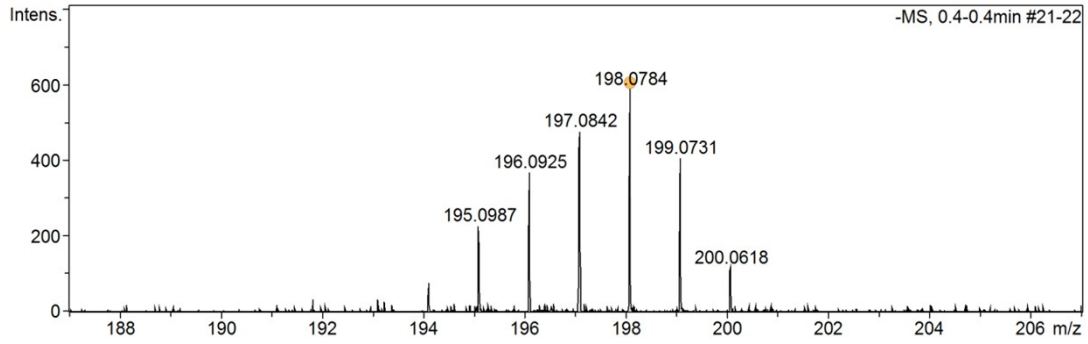

Figure S31. Mass spectrum of Na[closo-1-CHB_9H_8-6-Br] in methanol. HRMS (negative mode ESI) *m/z*: $[M\text{-}Na]^-$ calcd. for $CHB_9H_8Br^-$ 198.0786; found 198.0784

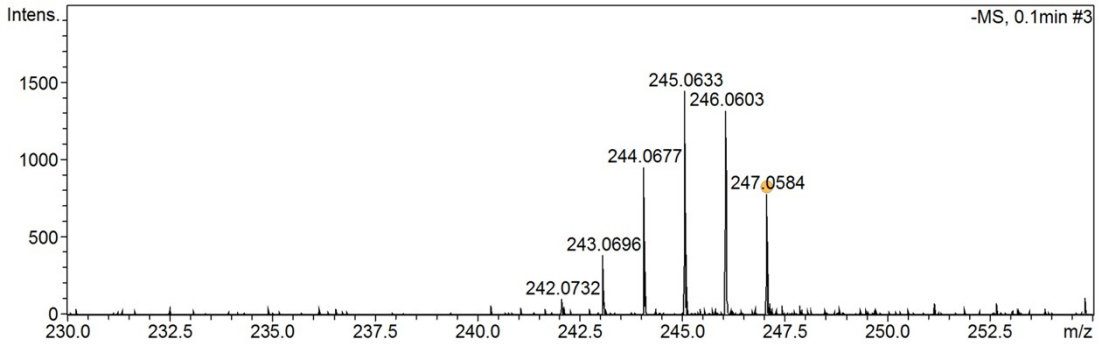

Figure S32. Mass spectrum of Na[*closo*-1-CHB_9H_8-6-I] in methanol. HRMS (negative mode ESI) *m/z*: $[M\text{-}Li]^-$ calcd. for $CHB_9H_8I^-$ 245.0665; found 245.0633.

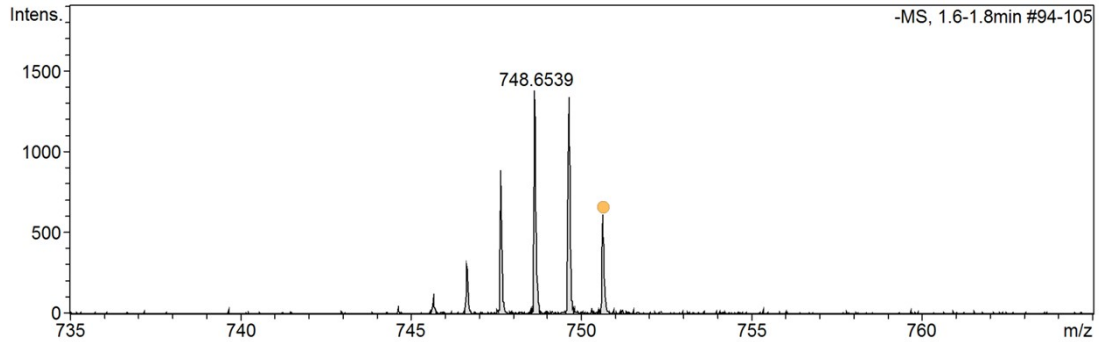

Figure S33. Mass spectrum of Na[*closo*-1-CHB_9H_4-6,7,8,9,10-I_5] in methanol. HRMS (negative mode ESI) *m/z*: $[M\text{-}Na]^-$ calcd. for $CHB_9H_4I_5^-$ 748.6530; found 748.6539.

Figure S34. Mass spectrum of Li[closo-1-CHB_9H_8-6-Br] in methanol. HRMS (negative mode ESI) *m/z*: $[M\text{-}Li]^-$ calcd. for $CHB_9H_8Br^-$ 198.0786; found 198.0784

Figure S35. Mass spectrum of Li[*closo*-1-CHB_9H_8-6-I] in methanol. HRMS (negative mode ESI) *m/z*: $[M\text{-}Li]^-$ calcd. for $CHB_9H_8I^-$ 245.0665; found 245.0633.

Figure S36. Mass spectrum of Li[*closo*-1-CHB_9H_4-6,7,8,9,10-I_5] in methanol. HRMS (negative mode ESI) *m/z*: $[M\text{-}Li]^-$ calcd. for $CHB_9H_4I_5^-$ 748.6530; found 748.6539.

FTIR Spectra (Figures S37-S38)

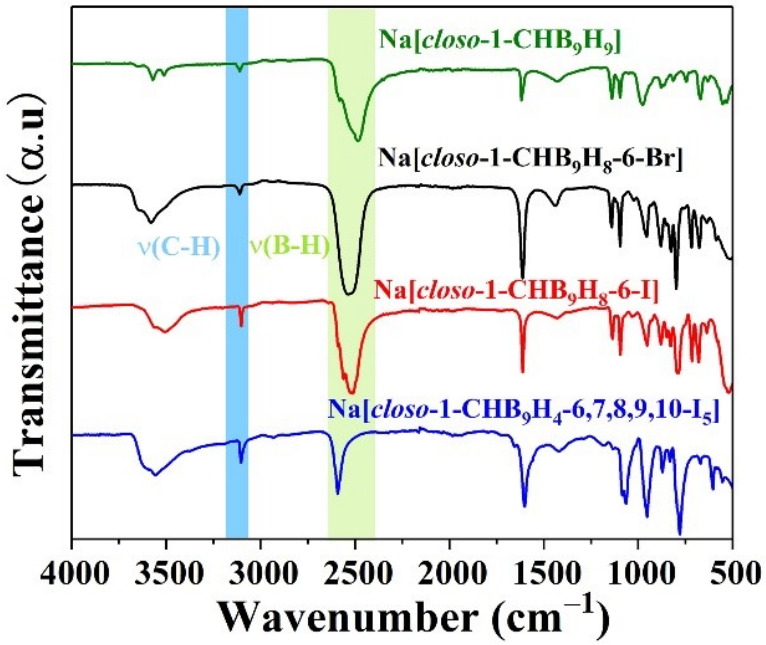

Figure S37. FTIR spectra of the Na[*closo*-1-CHB$_9$H$_9$], Na[*closo*-1-CHB$_9$H$_8$-6-Br], Na[*closo*-1-CHB$_9$H$_8$-6-I] and Na[*closo*-1-CHB$_9$H$_4$-6,7,8,9,10-I$_5$] compounds

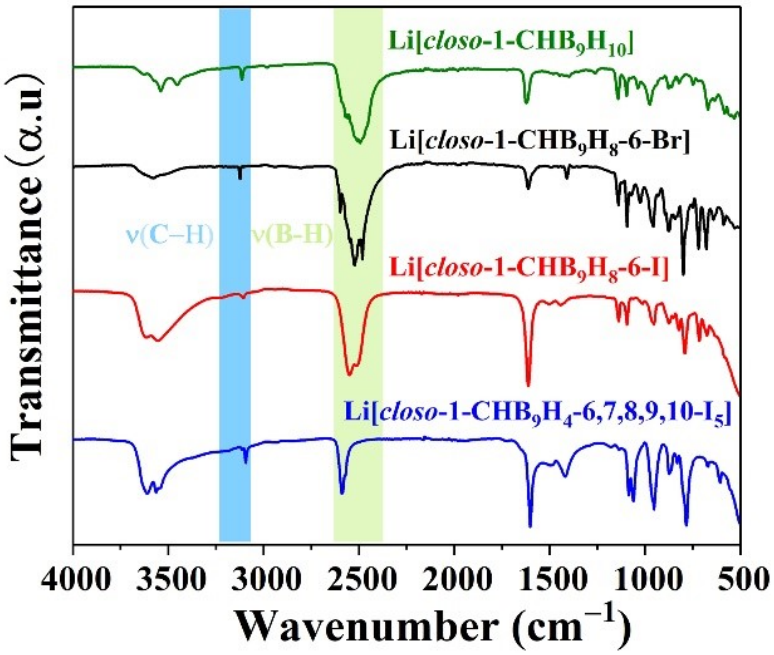

Figure S38. FTIR spectra of the Li[*closo*-1-CHB$_9$H$_9$], Li[*closo*-1-CHB$_9$H$_8$-6-Br], Li[*closo*-1-CHB$_9$H$_8$-6-I] and Li[*closo*-1-CHB$_9$H$_4$-6,7,8,9,10-I$_5$] compounds

Table S1. Characteristic IR frequencies (cm^{-1}) of the M[*closo*-1-CHB_9H_9], M[*closo*-1-CHB_9H_8-6-Br], M[*closo*-1-CHB_9H_8-6-I] and M[*closo*-1-CHB_9H_4-6,7,8,9,10-I_5] (M = Li, Na) compounds

Li[*closo*-1-CHB_9H_9]	3114(w), 2498(s), 1406(w), 1139(m), 1094(s),
Li[*closo*-1-CHB_9H_8-6-Br]	3127(w), 2508(s), 1406(w), 1144(m), 1094(s),
Li[*closo*-1-CHB_9H_8-6-I]	3109(w), 2526(s), 1448(w), 1146(m), 1096(s),
Li[*closo*-1-CHB_9H_4-6,7,8,9,10-I_5]	3091(w), 2590(s), 1420(w), 1084(m), 1061(s),
Na[*closo*-1-CHB_9H_9]	3105(w), 2485(s), 1424(w), 1139(m), 1096(s),
Na[*closo*-1-CHB_9H_8-6-Br]	3105(w), 2530(s), 1443(w), 1145(m), 1090(s),
Na[*closo*-1-CHB_9H_8-6-I]	3105(w), 2522(s), 1424(w), 1142(m), 1094(s),
Na[*closo*-1-CHB_9H_4-6,7,8,9,10-I_5]	3100(w), 2590(s), 1433(w), 1080(m), 1061(s),

Note: characteristic peaks at about 3500 and 1600 cm^{-1} are assigned to water.

^{11}B NMR spectra of M[*closo*-1-CHB_9H_8-6-X] (M = Na, Li; X = Br, I) and M[*closo*-1-CHB_9H_4-6, 7, 8, 9, 10-I_5] (M = Na, Li) recorded after heating to a given temperature

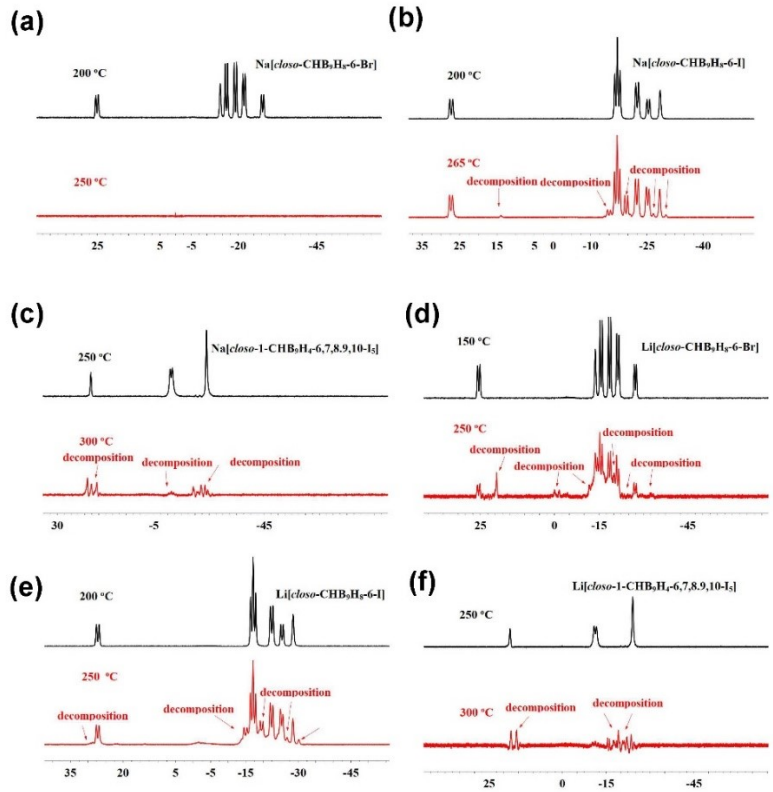

Figure S39. ^{11}B NMR spectra of (a) Na[*closo*-1-CHB_9H_8-6-Br], (b) Na[*closo*-1-CHB_9H_8-6-I], (c) Na[*closo*-1-CHB_9H_4-6,7,8,9,10-I_5], (d) Li[*closo*-1-CHB_9H_8-6-Br], (e) Li[*closo*-1-CHB_9H_8-6-I], and (f) Li[*closo*-1-CHB_9H_4-6,7,8,9,10-I_5] recorded after heating to given temperature.

FTIR Spectra of M[*closo*-1-CHB_9H_4-6,7,8,9,10-I_5] (M = Na, Li) recorded before and after heated to 300 °C

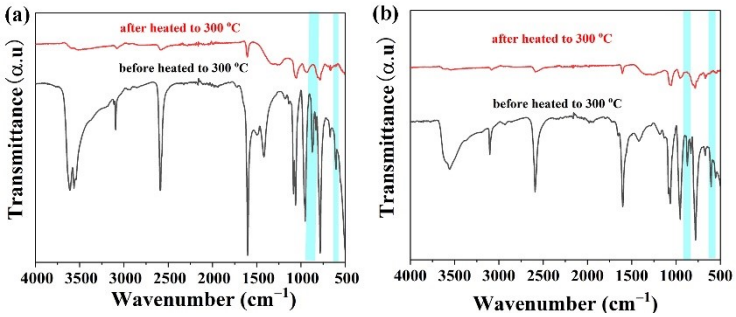

Figure S40. FTIR spectra of (a) Na[*closo*-1-CHB_9H_4-6,7,8,9,10-I_5] and (b) Li[*closo*-1-CHB_9H_4-6,7,8,9,10-I_5] recorded before and after heated to 300 °C.

Photographs of the pellet of Na[*closo*-1-CHB_9H_8-6-I] after heating to a given temperature

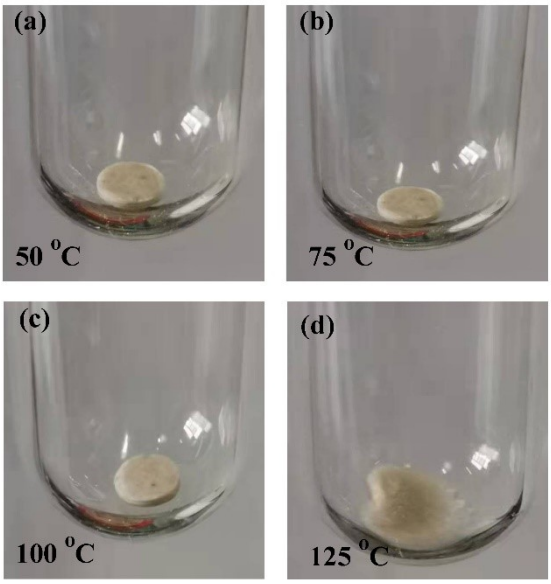

Figure S41. Photographs of the pellet of Na[*closo*-1-CHB_9H_8-6-I] after heating to a given temperature: (a) 50, (b) 75, (c) 100, and (d) 125 °C.

Activation energies of the Na[*closo*-1-$CHB_9H_{9-n}X_n$] (n = 0; n = 1, X = Br, I; n = 5, X = I) and Li[*closo*-1-$CHB_9H_{9-n}X_n$] (n = 0; n = 1, X = Br, I; n = 5, X = I)

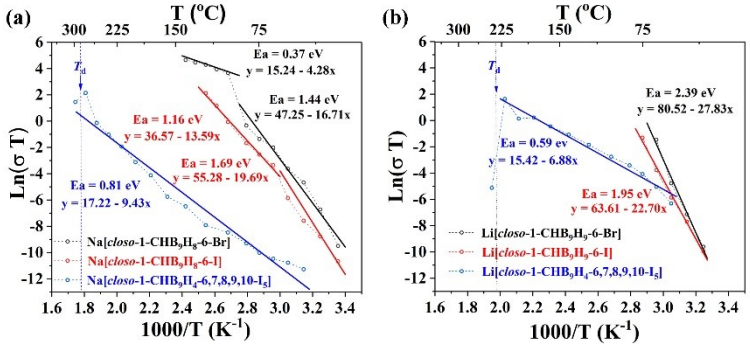

Figure 42. (a) Activation energies of the Na[*closo*-1-$CHB_9H_{9-n}X_n$] (n = 0; n = 1, X = Br, I; n = 5, X = I); (b)Activation energies of the Li[*closo*-1-$CHB_9H_{9-n}X_n$] (n = 0; n = 1, X = Br, I; n = 5, X = I)